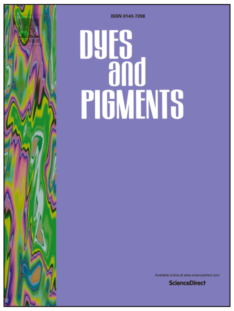

Hexa-substituted benzene derivatives as hole transporting materials for efficient perovskite solar cells

Yuan Liu, Chen Tao, Guohua Xie, Jeroen Van Der Velden, Sergio Marras, Zhenghui Luo, Xuan Zeng, Annamaria Petrozza, Chuluo Yang

PII: S0143-7208(18)31992-2

DOI: https://doi.org/10.1016/j.dyepig.2018.12.010

Reference: DYPI 7215

To appear in: *Dyes and Pigments*

Received Date: 8 September 2018

Revised Date: 24 October 2018

Accepted Date: 6 December 2018

Please cite this article as: Liu Y, Tao C, Xie G, Van Der Velden J, Marras S, Luo Z, Zeng X, Petrozza A, Yang C, Hexa-substituted benzene derivatives as hole transporting materials for efficient perovskite solar cells, *Dyes and Pigments* (2019), doi: https://doi.org/10.1016/j.dyepig.2018.12.010.

MS Title: Hexa-substituted benzene derivatives as hole transporting materials for efficient perovskite solar cells

Authors: *Yuan Liu, Chen Tao, Guohua Xie, Jeroen Van Der Velden, Sergio Marras, Zhenghui Luo, Xuan Zeng, Annamaria Petrozza and Chuluo Yang*

Graphical Abstract

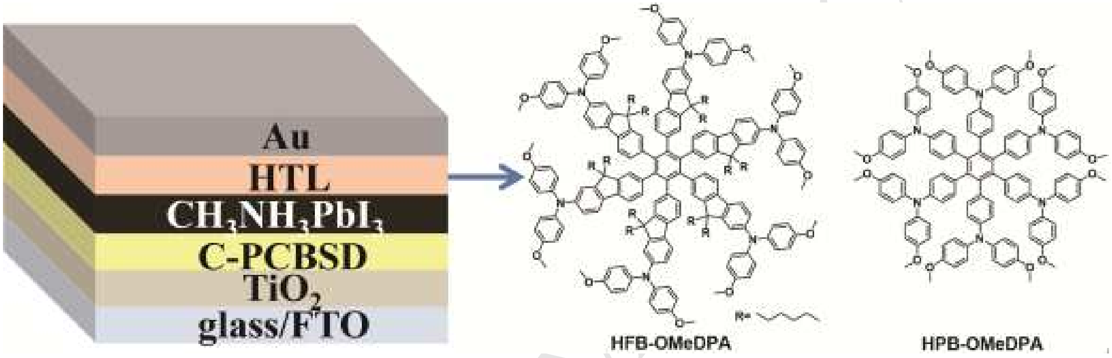

Two hexa-substituted benzene compounds have been successfully utilized as efficient hole transporting materials (HTMs) for high performance perovskite solar cells. The relationships between molecular structure, electronic properties of the semiconductor and eventually the photovoltaic performance are investigated. Both compounds exhibit good solubility, excellent thermal stability, high hole mobility and suitable energy levels. Perovskite solar cells employed these two HTMs exhibit impressive PCEs of 15.9% and 16.7%, respectively, which are comparable to the reference cells based on spiro-OMeTAD.

Hexa-substituted benzene derivatives as hole transporting materials for efficient perovskite solar cells

Yuan Liu[a,1], Chen Tao[c,1,*], Guohua Xie[b], Jeroen Van Der Velden[c], Sergio Marras[d], Zhenghui Luo[b], Xuan Zeng[b], Annamaria Petrozza[c] and Chuluo Yang[b,*]

[a] *School of Chemical Engineering and Light Industry, Guangdong University of Technology, Guangzhou 510006, China.*

[b] *Hubei Key Lab on Organic and Polymeric Optoelectronic Materials, Department of Chemistry, Wuhan University, Wuhan 430072, China.*

[c] *Center for Nano Science and Technology @PoliMi, Istituto Italiano di Tecnologia, via Giovanni Pascoli 70/3, 20133 Milan, Italy.*

[d] *Department of Nanochemistry, Istituto Italiano di Tecnologia via Morego 30, 16163 Genova, Italy.*

[1] *These authors contributed equally to this work.*

* *Corresponding author, E-mail: clyang@whu.edu.cn (C. Yang); taochen635@whu.edu.cn (C. Tao)*

Abstract

Two low cost hexa-substituted benzene derivatives, namely HFB-OMeDPA and HPB-OMeDPA, have been successfully utilized as hole transporting materials (HTMs) for efficient perovskite solar cells (PSCs). The relationships between molecular structure, electronic properties of the semiconductor and eventually the photovoltaic performance are investigated. The planar PSCs employing HPB-OMeDPA as HTM exhibit excellent power conversion efficiencies exceeding 16% under AM 1.5G illumination conditions, which are comparable to the reference cells based on spiro-OMeTAD.

Keywords: Hole transporting material; Hexa-substituted; Perovskite solar cell; Low cost

1. Introduction

Organic-inorganic metal halide perovskite solar cells (PSCs) have attracted significant attention in the field of photovoltaics due to the boosting power conversion efficiencies (PCEs) exceeding 22% during the past few years [1-4]. The superior photovoltaic performances of PSCs originate from the unique opto-electronic properties of perovskite, such as direct bandgap, ambipolar charge mobilities, long carrier diffusion lengths, high extinction coefficient in a wide absorption range [5-8]. Many efforts have been devoted to the optimization of PSCs, including device architectures, the quality of perovskite films, and interfacial engineering, e.g., the charge transport materials between perovskites and electrodes [9]. The hole transporting materials (HTMs) that transfer holes from the perovskite layer to the hole-collecting electrodes and reduce the electron-hole recombination by blocking the electrons, play crucial roles in achieving high performance PSCs. Ideal HTMs are required to have appropriate energy levels, high hole mobility and conductivity, solution processibility, low cost and reproducibility. In this regard, small molecular HTMs possessing dominant advantages over inorganic semiconductors or polymers are deliberately designed. The state-of-the-art small molecule, (2,2',7,7'-tetrakis[*N*,*N*-di-*p*-methoxyphenylamine]-9,9'-spirobifluorene) (spiro-OMeTAD), is the most commonly used and efficient HTM in PSCs [10-12]. However, the complicated synthesis and purification procedures make it expensive and, therefore, limit its practical applications in PSCs and hence the future commercialization.

Significant efforts have been dedicated towards designing and synthesizing new HTMs [13-15]. A large number of small molecular HTMs based on ethylenedioxythiophene, cruciform oligothiophenes, pyrene, triptycene, triazines, conjugated quinolizino acridine, planar triphenylamine, furan, silolothiophene, carbazole, tetrathiafulvalene, phenoxazine, paracyclophane and ethene-tetraarylamine cores have been reported [13-28]. Although the device performances based on these HTMs are similar to or even superior than those of the devices with spiro-OMeTAD in some aspects, there still remains a concern of commercialization when taking cost, efficiency and stability into consideration. Besides, the relationships between molecular structures and hole-transport properties as well as the photovoltaic performances are not fully addressed. In this regard, further exploration of advanced HTMs is significant to both industry and academia.

Star-shaped molecules typically comprise a central core and multiple conjugated arms as the functional groups. Owing to the well-defined structure with precise molecular weights, star-shaped molecules combine the advantages of both small molecules and polymers, such as good thermal stability, well film-forming property, and good reproducibility [29-31]. The 3D structure of spiro-OMeTAD has been widely investigated, in which four dimethoxydiphenylamine units attach to the spiro core. Similar to the spiro-OMeTAD, the HTMs with different numbers of the attaching arms have been discussed as well [32,33]. It is well known that their photophysical, electrochemical, thermal properties as well as the hole mobilities strongly rely on the central core, the linkage bridge and the numbers of arms. However, the effect of multi-armed, *e.g.* hexa-substituted molecules have rarely been reported. It should be noted that during the preparation of this manuscript, Bo and his coworkers just published their research of one flower-shaped molecule as HTM for perovskite solar cells, which is identical to our study [34]. The hexarylbenzene-based compounds possess sterically crowded structures, in which six aryl groups are grafted onto the central benzene core and can be readily modified on the peripheral aryl groups.

In this work, two hexarylbenzene-based compounds with six dimethoxydiphenylamine groups linked by fluorenyl or phenyl bridges attaching to the central benzene core, namely 7,7',7'',7''',7'''',7'''''-(phenyl-1,2,3,4,5,6-hexakis(9,9-dihexyl)-*N*,*N*-bis(4-methoxyphenyl)-9*H*-fluoren-2-amine) (HFB-OMeDPA) and 1,2,3,4,5,6- hexakis(((4-methoxyphenyl)amine)phenyl)benzene (HPB-OMeDPA), are synthesized (Scheme 1). The hydrotropy dimethoxydiphenylamine units and additional flexible alkyl chains allow both compounds with extremely high solubility. Moreover, owing to the different linkage bridges, these two compounds exhibit different photophysical, electrochemical, thermal and hole transport properties. The PSCs employing these compounds as HTMs deliver average conversion efficiencies of 15.4% and 16.4%, respectively, which are comparable to the efficiency of the controlled device with spiro-OMeTAD of 17.1%. We show that the additional flexible alkyl chains in the HFB-OMeDPA influence the packing mode in solid state, resulting in a relatively lower hole mobility. The photoluminescence quenching indicates that the hole transfer from perovskites to both HPB-OMeDPA and HFB-OMeDPA is comparably efficient to the spiro-OMeTAD case. These results demonstrate that the design of linkage bridges in the hexarylbenzene-based compounds are particularly important, and provide a fundamental understanding for further optimizing HTMs for PSCs.

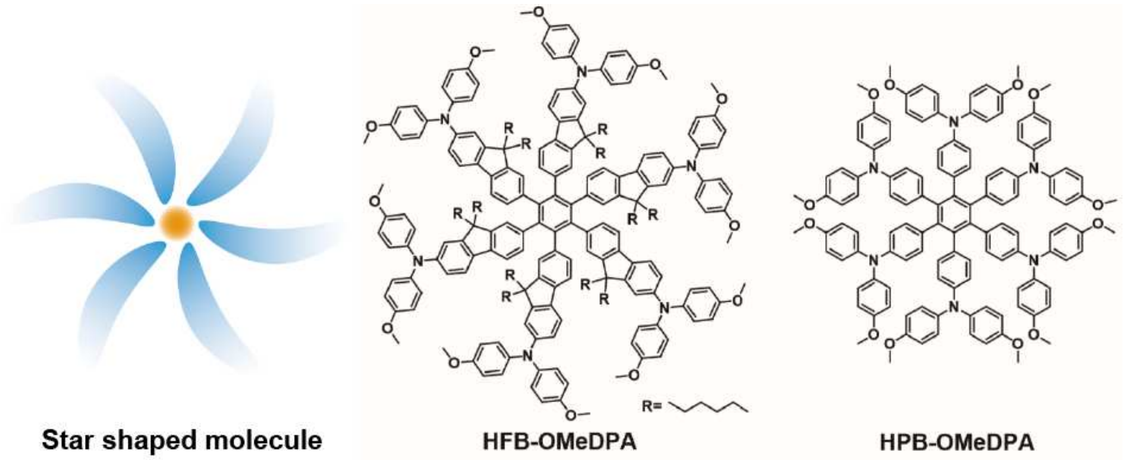

Scheme 1. Chemical structures of HFB-OMeDPA and HPB-OMeDPA.

2. Results and discussion

2.1 Synthesis and characterization

The synthetic routes of the two compounds are depicted in Scheme S1, and the detailed synthetic procedures are provided in the supporting information. The key intermediate of 1,2,3,4,5,6-hexakis(7-bromo-9,9-dihexyl-9*H*-fluoren-2-yl)benzene (1) was synthesized *via* cyclotrimerisation of diarylethyne catalyzed by dicobaltoctacarbonyl [30]. Another key intermediate of hexakis(4-bromophenyl)benzene (2) was readily prepared from hexaphenylbenzene by bromination using neat bromine [35]. The final products of HFB-OMeDPA and HPB-OMeDPA were obtained by the Buchwald-Hartwig coupling reaction of 1 or 2 with 4,4'-dimethoxydiphenylamine with over 70% yield. The structures of HFB-OMeDPA and HPB-OMeDPA were fully characterized by ^{1}H NMR, ^{13}C NMR, mass spectrometry and elemental analysis, and the data were all in good agreement with the designed structures. Moreover, owing to the peripheral dimethoxydiphenylamine units and additional flexible alkyl chains, all the compounds exhibit excellent solubility in the common solvents, such as chloroform and chlorobenzene. The lab synthesis costs of HFB-OMeDPA and HPB-OMeDPA are estimated at 12.95 US$ g^{-1} and 10.27 US$ g^{-1}, respectively, which are approximately a tenth of the costs of purified spiro-OMeTAD [36]. The detailed costs are listed in Table S1.

2.2 DFT calculation

To estimate the frontier molecular orbitals of the designed molecules, the density functional theory (DFT) calculations were performed. The HOMO and LUMO distributions for the optimized ground-state geometries of these molecules are shown in Fig. 1. The HOMO of HFB-OMeDPA is uniformly distributed over the molecule, while the HOMO of HPB-OMeDPA is located in one arm. For both molecules, the six arms are highly twisted with respect to the benzene ring in order to alleviate the steric hindrance. The respective dihedral angles between these two planes are 66.2° for HFB-OMeDPA and 61.2° for HPB-OMeDPA. Owing to the relatively larger dihedral angle, HFB-OMeDPA exhibits lower conjugation degree than HPB-OMeDPA. Besides, the flexible alkyl chains in the fluorenyl bridge of HFB-OMeDPA are free from the molecule plane, which inhibits the molecular packing and weakens the intermolecular interaction.

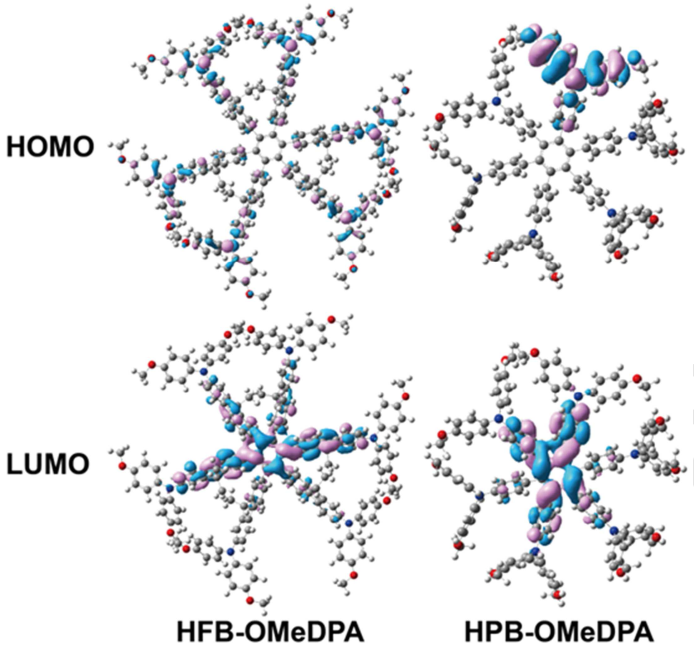

Fig. 1. The HOMO and LUMO distributions of HFB-OMeDPA and HPB-OMeDPA using DFT calculations.

2.3 Photophysical, electrochemical and thermal properties

UV-Vis absorption spectra of HFB-OMeDPA and HPB-OMeDPA in dichloromethane and neat films are illustrated in Fig. 2a. Both compounds show intense π-π^* absorption bands that mainly locate in the UV range. The nearly optical transparency of these two compounds in visible and near infrared region leads to negligible parasitic absorption in a solar cell. The absorption maximum is 306 nm for HPB-OMeDPA. It shifts to 360 nm for HFB-OMeDPA in that the π bridge changes from phenyl to fluorenyl unit. HFB-OMeDPA exhibits analogical absorption spectra in solution and films. However, the absorption maximum of HPB-OMeDPA films (314 nm) appears a slight redshift compared to that in dichloromethane, which indicates the emergence of stronger intermolecular interaction originated from the π-π stacking in solid state. The absorption spectra of spiro-OMeTAD in dichloromethane and neat film are carried out for comparation. Calculated from the onsets of the optical absorption spectra, the energy gaps (E_gs) of HFB-OMeDPA, HPB-OMeDPA and spiro-OMeTAD are estimated to be 3.05, 3.19 and 2.98 eV, respectively. The UV/Vis absorption spectra of HTMs and dopants (4-*tert*-butylpyridine and lithium bis(trifluoromethylsulphonyl)imide) in films are illustrated in Fig. S1. The doped HTMs exhibit slightly higher absorbance in the range of 250~270 nm than the respective undoped HTMs, which might be attributed to the absorption of 4-*tert*-butylpyridine.

The electrochemical properties of these compounds are investigated by cyclic voltammetry (CV) measurements. As shown in Fig. 2b, all compounds display reversible oxidation behavior in dichloromethane, which can be assigned to the oxidation of peripheral dimethoxydiphenylamine moieties. HFB-OMeDPA, HPB-OMeDPA and spiro-OMeTAD exhibit the onset of oxidation potential of 0.57, 0.60 and 0.47 V, respectively. Considering the onset of oxidation potential (0.48 V in dichloromethane) and vacuum energy level (-5.1 eV) of ferrocene [37], the HOMO levels are established to be -5.19, -5.22 and -5.09 eV for HFB-OMeDPA, HPB-OMeDPA and spiro-OMeTAD, respectively. Deduced from the optical E_gs and HOMO levels, the respective LUMO levels are -2.32, -2.32 and -2.11 eV. It should be noted that HFB-OMeDPA and HPB-OMeDPA show no overlapped oxidation waves assigned to the through-space interaction between arms. This implies that the hole wavefunction is delocalized over peripheral dimethoxydiphenylamine moieties and the arms are independent to each other [29]. The HOMO levels of HFB-OMeDPA and HPB-OMeDPA match well with the valence band (VB) of $CH_3NH_3PbI_3$ (-5.43 eV) and the work function of Au (-5.0 eV), thereby favoring the hole transfer at $CH_3NH_3PbI_3$/HTM interface. Besides, the LUMO levels of both compounds are higher than the conduction band (CB) of $CH_3NH_3PbI_3$ (-3.92 eV), which could block the electron transfer from perovskite to anode (Au) and hence suppress interfacial charge recombination.

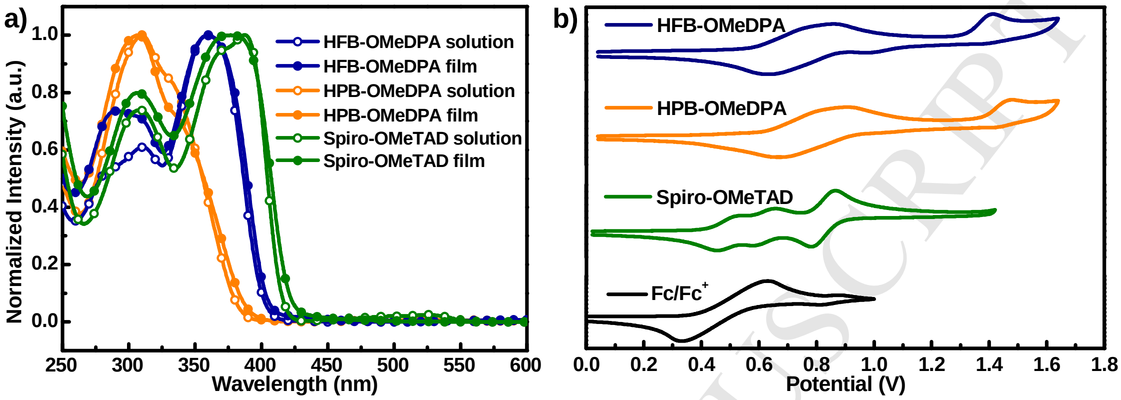

Fig. 2. a) UV/Vis absorption spectra of HFB-OMeDPA, HPB-OMeDPA and spiro-OMeTAD in dichloromethane and neat films, respectively. b) Cyclic voltammograms of HFB-OMeDPA, HPB-OMeDPA and spiro-OMeTAD in dichloromethane for oxidation, respectively.

The thermal properties of HFB-OMeDPA and HPB-OMeDPA are investigated by thermogravimetric analysis (TGA) and differential scanning calorimetry (DSC). As shown in Fig. S2, both compounds exhibit high decomposition temperatures (T_d) of above 420 ^oC, which are close to that of spiro-OMeTAD (445 ^oC) and far above temperatures for conventional device operation [36]. The glass transition temperatures (T_gs) for HFB-OMeDPA and HPB-OMeDPA are 199 and 160 ^oC, respectively, which are both higher than that of spiro-OMeTAD (120 ^oC) [35]. The high T_gs are mainly ascribed to the rigidity of the hexarylbenzene architecture, in which six bulky arms grafted onto single benzene prohibit the free rotation of the arms. The good thermal stability of HFB-

OMeDPA and HPB-OMeDPA are favored for the lifetime of perovskite solar cells in operation.

2.4 Hole transporting property

In order to gain more insight into the hole transporting properties of HFB-OMeDPA and HPB-OMeDPA, we carry out space-charge-limited current (SCLC) measurements with the hole-only device configuration of ITO/PEDOT:PSS/HTM/Au. As shown in Fig. S3, the hole mobility of each compound was determined by fitting the current density-voltage (*J*-*V*) curves to the Mott-Gurney law (Equation S1). The hole mobility of spiro-OMeTAD was measured under the same experimental conditions for comparison, and evaluated to be (8.42 ± 1.44) x 10^{-4} cm^2 V^{-1} s^{-1}. The hole mobility of HPB-OMeDPA is comparable to that of spiro-OMeTAD, and one order of magnitude higher than that of HFB-OMeDPA. The calculated hole mobilities of HFB-OMeDPA and HPB-OMeDPA are (5.54 ± 0.62) x 10^{-5} and (7.38 ± 1.12) x 10^{-4} cm^2 V^{-1} s^{-1}, respectively. Notably, HFB-OMeDPA exhibits distinct light-soaking effect. Its hole mobility increases and reaches up to 1.65 x 10^{-4} cm^2 V^{-1} s^{-1} upon light soaking. The higher hole mobility of HPB-OMeDPA should be attributed to the π-π stacking in solid state, which facilitates efficient intermolecular charge transfer. However, the flexible alkyl chains in the fluorenyl bridge of HFB-OMeDPA inhibit the aggregation of the molecules, resulting in relatively low hole mobilities. The detailed parameters of HFB-OMeDPA and HPB-OMeDPA are summarized in Table 1.

Table 1. Photophysical, electrochemical, thermal parameters and hole mobilities of HFB-OMeDPA and HPB-OMeDPA.

HTM	λ_{abs}[a]/ λ_{abs}^{film} [nm]	E_g[b] [eV]	HOMO[c] /LUMO[d] [eV]	T_d/T_g[e] [°C]	μ_h[f] [$cm^2\ V^{-1}\ s^{-1}$]
HFB-OMeDPA	360/360	3.05	-5.19/-2.14	465/199	$(5.54 \pm 0.62) \times 10^{-5}$
HPB-OMeDPA	306/314	3.19	-5.22/-2.03	420/160	$(7.38 \pm 1.12) \times 10^{-4}$
spiro-OMeTAD	387/376	2.98	-5.09/-2.11	-/-	$(8.42 \pm 1.44) \times 10^{-4}$

[a]Measured in DCM solution. [b]Calculated from the edge of the long wavelength absorption. [c]Determined from the onset of oxidation potentials. [d]Deduced from HOMO and E_g. [e]Obtained from TGA and DSC measurements (T_d, corresponding to 5% weight loss). [f]Measured in the space-charge limited current (SCLC) regime and fitted using the Mott-Gurney law.

2.5 Photoluminescence spectroscopy

Fig. 3a shows the normalized photoluminescence (PL) spectra of $CH_3NH_3PbI_3$ films with and without HTM deposited on glass substrates. The excitation wavelength was 460 nm that was beyond the HTM absorption spectra (shown in Fig. 2a). The pristine perovskite sample exhibits a distinct PL emission peaking at 775 nm. After the incorporation of different HTM layers, the PL significantly quenches. The PL quenching degree increases as the order of HFB-OMeDPA<HPB-OMeDPA<spiro-OMeTAD (shown in insert Fig. 3a).

The charge dynamics of the perovskite layer with and without HTMs are investigated with time-resolved PL (TR-PL) measurements. The signals have been collected at 775 nm, where $CH_3NH_3PbI_3$ films peak. The pristine $CH_3NH_3PbI_3$ show a long-living signal. As shown in Fig. 3b, the fitting lifetime for the pristine $CH_3NH_3PbI_3$ film was 93.9 ns.

However, the decay lifetimes of the $CH_3NH_3PbI_3$/HTM bilayer are found to be significantly reduced. The lifetimes progressively shorten to be 10.1, 7.1 and 4.6 ns for perovskites covered with HFB-OMeDPA, HPB-OMeDPA and spiro-OMeTAD, respectively. This suggest that an efficient hole transfer is established at the $CH_3NH_3PbI_3$/HTM interface.

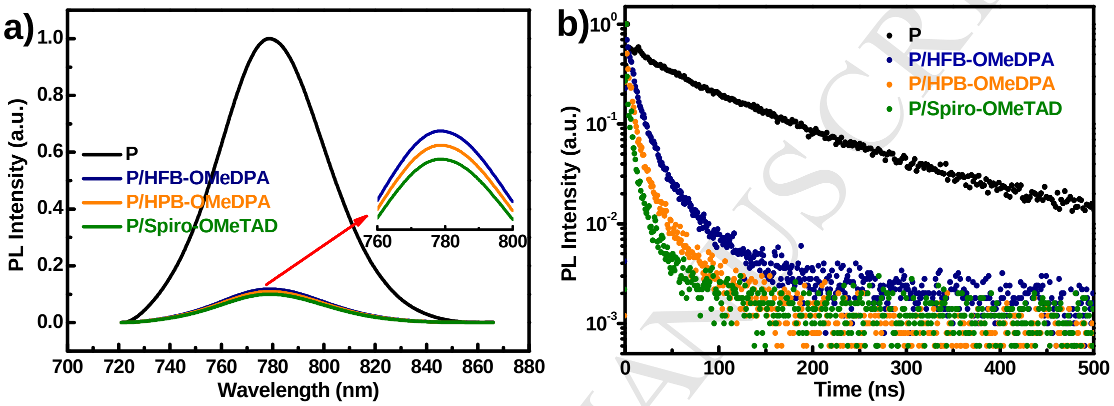

Fig. 3. a) The steady-state photoluminescence (PL) spectra and b) time-resolved PL spectra of $CH_3NH_3PbI_3$, $CH_3NH_3PbI_3$/HFB-OMeDPA, $CH_3NH_3PbI_3$/HPB-OMeDPA and $CH_3NH_3PbI_3$/spiro-OMeTAD.

2.6 Device performance

We use HFB-OMeDPA, HPB-OMeDPA and spiro-OMeTAD to fabricate planar perovskite solar cells. Fig. 4 shows the cross-sectional scanning electron microscopy (SEM) images of a full device stack with $MAPbI_3$. The planar perovskite solar cells with different HTMs were fabricated with TiO_2/crosslinked [6,6]-phenyl-C_{61}-butyric styryl dendron ester (C-PCBSD) as the electron transport layer. Tao et al. had shown that the incorporation of C-PCBSD at TiO_2/perovskite interface not only facilitates perovskite grain growth but also significantly prohibit charge recombination [38]. The optimized thicknesses of HFB-OMeDPA and HPB-OMeDPA are both ~100 nm, which is slightly below the optimized thickness for spiro-OMeTAD of ~150 nm. Lithium bis(trifluoromethylsulfonyl)-imide (Li-TFSI) and 4-*tert*-butyl pyridine (*t*-BP) are the additives for all the HTMs (detailed information can be found in supplementary information).

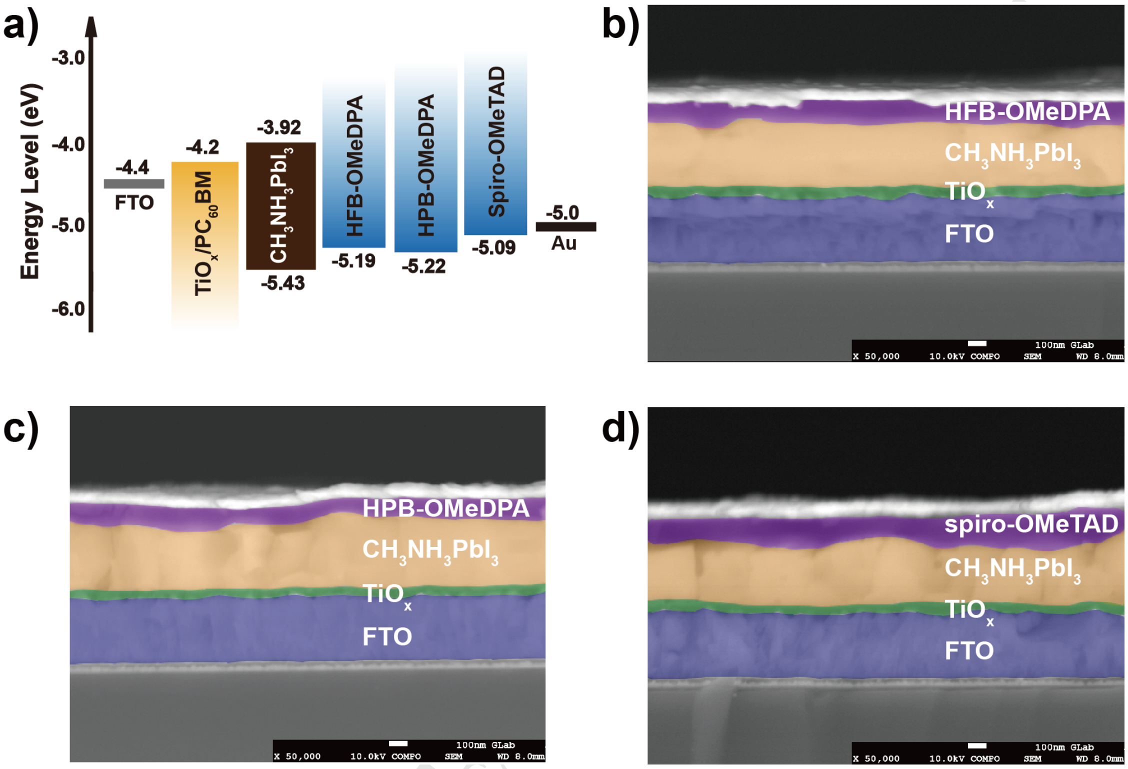

Fig. 4. a) Energy level diagrams of the used materials. SEM cross section of photovoltaic cells based on HFB-OMeDPA b), HPB-OMeDPA c) and spiro-OMeTAD d), respectively. The scale bar is 100 nm.

Fig. 5 presents the current density versus voltage (*J*-*V*) characteristics of our champion devices measured in air under air mass 1.5 global (AM 1.5G) conditions with a slow scan rate of 0.023 V s^{-1}. The corresponding photovoltaic parameters, such as short-circuit current density (J_{SC}), open-circuit voltage (V_{OC}), fill factor (FF), and PCE, are summarized in Table 2. For comparison, the spiro-OMeTAD-based device exhibits the best performance among them, reaching an average PCE of 17.1% with a V_{OC} of 1.10 V, a J_{SC} of 21.2 mA cm^{-2}, a FF of 73.1%. The HFB-OMeDPA-based devices yielded a V_{OC} of 1.09 V, a J_{SC} of 19.9 mA cm^{-2}, a FF of 71.4%, leading to an average PCE of 15.4%. The HPB-OMeDPA based device exhibited a V_{OC} of 1.09 V, a J_{SC} of 20.3 mA cm^{-2} and a FF of 73.5%, resulting in an average PCE of 16.4%.

The external quantum efficiency (EQE) spectra of the PSCs with different HTMs were recorded and shown in Fig. 5d. The integrated J_{sc}s calculated from the EQE spectra were 19.2, 19.3, and 20.1 mA cm^{-2} for HFB-OMeDPA, HPB-OMeDPA, and spiro-OMeTAD, respectively, which is in agreement with those obtained from *J-V* curves. The EQE values maintain above 70% in the range of 450-750 nm, which indicates the efficient light harvesting and photon-to-electron conversion.

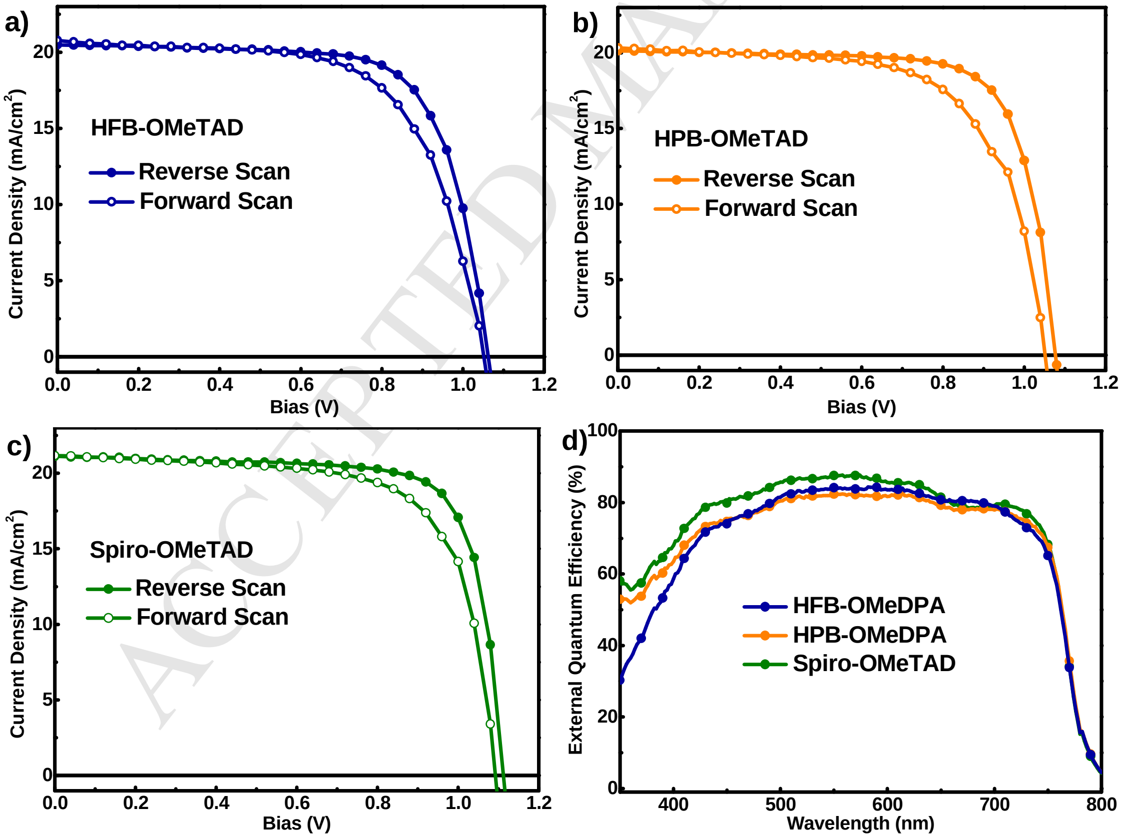

Fig. 5. J-V characteristics of PSCs utilizing a) HFB-OMeDPA, b) HPB-OMeDPA and c) spiro-OMeTAD as HTMs with a scan rate of 0.023 V s^{-1}, d) EQE spectra of PSCs based on different HTMs.

Table 1. Photovoltaic parameters of the champion PSCs with different HTMs. (scanning rate: 0.023 V s^{-1})

HTM	Scan direction	V_{OC} (V)	J_{SC} (mA cm^{-2})	FF (%)	PCE (%)
HFB-OMeDPA	Reverse	1.09	19.8	73.8	15.9
	Forward	1.08	19.9	69.0	14.9
	Average	1.09	19.9	71.4	15.4
HPB-OMeDPA	Reverse	1.09	20.3	75.4	16.7
	Forward	1.09	20.3	71.6	16.0
	Average	1.09	20.3	73.5	16.4
Spiro-OMeTAD	Reverse	1.11	21.1	76.4	18.0
	Forward	1.09	21.2	69.8	16.2
	Average	1.10	21.2	73.1	17.1

We have been able to repeat these results over several batches as demonstrated by the device statistics in Figs. S4 and S5 for HFB-OMeDPA and HPB-OMeDPA with 23 devices, respectively. The resulting device performances yield average PCEs of 14.1% ± 0.4% and 15.2% ± 0.3% for HFB-OMeDPA and HPB-OMeDPA based devices, respectively. The small deviations demonstrate the good reproducibility of the device performance based on these HTMs. The PCE difference is mainly ascribed to V_{OC} [(1.04 ± 0.02) V *vs* (1.07 ± 0.02) V] and FF (69.0 ± 3.8% vs 73.3% ± 1.6%). Thanks to the same device structure before HTM deposition, the microstructure and defect states in $MAPbI_3$ are not taken into consideration for the V_{OC} difference between devices with HFB-OMeDPA and HPB-OMeDPA. However, the abovementioned stronger intermolecular interaction in HPB-OMeDPA originated from the π-π stacking in solid state and hence higher hole mobility might account for the average higher V_{OC} in HPB-OMeDPA-based PSCs [39]. The average higher FF in the devices with HPB-OMeDPA might be related to the higher hole mobility of HPB-OMeDPA.

3. Conclusions

In summary, we have successfully demonstrated two hexarylbenzene-based compounds as efficient HTMs for high performance perovskite solar cells. These compounds are comprised of six dimethoxydiphenylamine units and benzene core, which are linked by fluorenyl or phenyl bridges, respectively. Both compounds exhibit good solubility, excellent thermal stability, high hole mobility and suitable energy levels. Perovskite solar cells employed these two HTMs exhibit impressive PCEs of 15.9% and 16.7%, respectively, which are comparable to the spiro-OMeTAD-based device. This work encourages us to further optimize the HTMs based on the hexa-substituted benzene derivatives, featuring considerably high performance and low cost.

Acknowledgements

We gratefully acknowledge financial support from the National Natural Science Foundation of China (Nos. 51703035, 21572171 and 61575146), and the Innovative Research Group of Hubei Province (No. 2015CFA014).

Appendix A. Supporting data

Supplementary data associated with this article can be found in the online version at http://dx.doi.org/

References

[1] Kojima A, Teshima K, Shirai Y, Miyasaka T. Organometal halide perovskites as visible-light sensitizers for photovoltaic cells. J Am Chem Soc 2009;131(17):6050-1.

[2] Correa-Baena J-P, Abate A, Saliba M, Tress W, Jesper Jacobsson T, Grätzel M, et al. The rapid evolution of highly efficient perovskite solar cells. Energy Environ Sci 2017;10(3):710-27.

[3] Samrana K, Khaja NM, Michael G, Shahzada A. Perovskite as Light Harvester: A game changer in photovoltaics. Angew Chem Int Ed 2014;53(11):2812-24.

[4] Research Cell Efficiency Records, NREL, https://www.nrel.gov/pv/assets/images/efficiency-chart.png, accessed July 2018.

[5] Stoumpos CC, Malliakas CD, Kanatzidis MG. Semiconducting tin and lead iodide perovskites with organic cations: phase transitions, high mobilities, and near-infrared photoluminescent properties. Inorg Chem 2013;52(15):9019-38.

[6] Stranks SD, Eperon GE, Grancini G, Menelaou C, Alcocer MJP, Leijtens T, et al. Electron-hole diffusion lengths exceeding 1 micrometer in an organometal trihalide perovskite absorber. Science 2013;342(6156):341-4.

[7] Xing G, Mathews N, Sun S, Lim SS, Lam YM, Grätzel M, et al. Long-range balanced electron- and hole-transport lengths in organic-inorganic $CH_3NH_3PbI_3$. Science 2013;342(6156):344-7.

[8] Noh JH, Im SH, Heo JH, Mandal TN, Seok SI. Chemical management for colorful, efficient, and stable inorganic-organic hybrid nanostructured solar cells. Nano Lett 2013;13(4):1764-9.

[9] Tao C, Neutzner S, Colella L, Marras S, Srimath Kandada AR, Gandini M, et al. 17.6% stabilized efficiency in low-temperature processed planar perovskite solar cells. Energy Environ Sci 2015;8(8):2365-70.

[10] Burschka J, Pellet N, Moon S-J, Humphry-Baker R, Gao P, Nazeeruddin MK, et al. Sequential deposition as a route to high-performance perovskite-sensitized solar cells. Nature 2013;499(7458):316-9.

[11] Liu D, Kelly TL. Perovskite solar cells with a planar heterojunction structure prepared using room-temperature solution processing techniques. Nat Photonics 2013;8:133-8.

[12] Jeon NJ, Lee HG, Kim YC, Seo J, Noh JH, Lee J, et al. o-Methoxy substituents in spiro-OMeTAD for Efficient inorganic-organic hybrid perovskite solar cells. J Am Chem Soc 2014;136(22):7837-40.

[13] Krishna A, Grimsdale AC. Hole transporting materials for mesoscopic perovskite solar cells - towards a rational design? J Mater Chem A 2017;5(32):16446-66.

[14] Calió L, Kazim S, Grätzel M, Ahmad S. Hole-transport materials for perovskite solar cells. Angew Chem Int Ed 2016;55(47):14522-45.

[15] Ameen S, Rub MA, Kosa SA, Alamry KA, Akhtar MS, Shin H-S, et al. Perovskite solar cells: influence of hole transporting materials on power conversion efficiency. ChemSusChem. 2015;9(1):10-27.

[16] Qin P, Paek S, Dar MI, Pellet N, Ko J, Grätzel M, et al. Perovskite solar cells with 12.8% efficiency by using conjugated quinolizino acridine based hole transporting material. J Am Chem Soc 2014;136(24):8516-9.

[17] Jeon NJ, Lee J, Noh JH, Nazeeruddin MK, Grätzel M, Seok SI. Efficient inorganic–organic hybrid perovskite solar cells based on pyrene srylamine ferivatives as hole-transporting materials. J Am Chem Soc 2013;135(51):19087-90.

[18] Shi Y, Hou K, Wang Y, Wang K, Ren H, Pang M, et al. Two methoxyaniline-substituted dibenzofuran derivatives as hole-transport materials for perovskite solar cells. J Mater Chem A 2016;4(15):5415-22.

[19] Park S, Heo JH, Cheon CH, Kim H, Im SH, Son HJ. A [2,2]paracyclophane triarylamine-based hole-transporting material for high performance perovskite solar cells. J Mater Chem A 2015;3(48):24215-20.

[20] Lim K, Kang M-S, Myung Y, Seo J-H, Banerjee P, Marks TJ, et al. Star-shaped hole transport materials with indeno[1,2-b] thiophene or fluorene on a triazine core for efficient perovskite solar cells. J Mater Chem A 2016;4(4):1186-90.

[21] Qin P, Kast H, Nazeeruddin MK, Zakeeruddin SM, Mishra A, Bauerle P, et al. Low band gap *S*,*N*-heteroacene-based oligothiophenes as hole-transporting and light absorbing materials for efficient perovskite-based solar cells. Energy Environ Sci 2014;7(9):2981-5.

[22] Abate A, Paek S, Giordano F, Correa-Baena J-P, Saliba M, Gao P, et al. Silolothiophene-linked triphenylamines as stable hole transporting materials for high efficiency perovskite solar cells. Energy Environ Sci 2015;8(10):2946-53.

[23] Zhu L, Shan Y, Wang R, Liu D, Zhong C, Song Q, et al. High-efficiency perovskite solar cells based on new TPE compounds as hole transport materials: the role of 2,7-and 3,6-substituted carbazole derivatives. Chem - Eur J 2017;23(18):4373-9.

[24] Krishna A, Sabba D, Li H, Yin J, Boix PP, Soci C, et al. Novel hole transporting materials based on triptycene core for high efficiency mesoscopic perovskite solar cells. Chem Sci 2014;5(7):2702-9.

[25] Do K, Choi H, Lim K, Jo H, Cho JW, Nazeeruddin MK, et al. Star-shaped hole transporting materials with a triazine unit for efficient perovskite solar cells. Chem Commun 2014;50(75):10971-4.

[26] Li H, Fu K, Hagfeldt A, Grätzel M, Mhaisalkar SG, Grimsdale AC. A Simple 3,4-ethylenedioxythiophene based hole-transporting material for perovskite solar cells. Angew Chem Int Ed 2014;53(16):4085-8.

[27] Gratia P, Magomedov A, Malinauskas T, Daskeviciene M, Abate A, Ahmad S, et al. A methoxydiphenylamine-substituted carbazole twin derivative: an efficient hole-transporting material for perovskite solar cells. Angew Chem Int Ed 2015;54(39):11409-13.

[28] Wang H, Sheikh AD, Feng Q, Li F, Chen Y, Yu W, et al. Facile synthesis and high performance of a new carbazole-based hole-transporting material for hybrid perovskite solar cells. ACS Photonics 2015;2(7):849-55.

[29] Kanibolotsky AL, Perepichka IF, Skabara PJ. Star-shaped π-conjugated oligomers and their applications in organic electronics and photonics. Chem Soc Rev 2010;39(7):2695-728.

[30] Yang Z, Ye T, Ma D, Qin J, Yang C. Star-shaped hexakis(9,9-dihexyl-9H-fluoren-2-yl)benzene end-capped with carbazole and diphenylamine units: solution-processable,

high *T*g hole-transporting materials for organic light-emitting devices. J Mater Chem 2012;22(44):23485-91.

[31] Yang Z, Jianhua Z, Tengling Y, Hao L, Chuluo Y, Hongbin W, et al. Unexpected propeller-like hexakis(fluoren-2-yl)benzene cores for six-arm star-shaped oligofluorenes: highly efficient deep-blue fluorescent emitters and good hole-transporting materials. Adv Funct Mater 2013;23(14):1781-8.

[32] Malinauskas T, Saliba M, Matsui T, Daskeviciene M, Urnikaite S, Gratia P, et al. Branched methoxydiphenylamine-substituted fluorene derivatives as hole transporting materials for high-performance perovskite solar cells. Energy Environ Sci 2016;9(5):1681-6.

[33] Park S, Jin HH, Yun JH, Jung TS, Kwak K, Min JK, et al. Effect of multi-armed triphenylamine-based hole transporting materials for high performance perovskite solar cells. Chem Sci 2016;7(8):5517-22.

[34] Kou C, Feng S, Li H, Li W, Li D, Meng Q, et al. Molecular "flower" as the high mobility hole transport material for perovskite solar cells. ACS Appl Mater Interfaces 2017;9(50):43855-60.

[35] Rathore R, Burns CL, Deselnicu MI. Multiple-electron transfer in a single step. Design and synthesis of highly charged cation-radical salts. Org Lett 2001;3(18):2887-90.

[36] Saliba M, Orlandi S, Matsui T, Aghazada S, Cavazzini M, Correabaena JP, et al. A molecularly engineered hole-transporting material for efficient perovskite solar cells. Nat Energy 2016;1(2):15017.

[37] Cardona CM, Li W, Kaifer AE, Stockdale D, Bazan GC. Electrochemical Considerations for Determining Absolute Frontier Orbital Energy Levels of Conjugated Polymers for Solar Cell Applications. Adv Mater 2011;23(20):2367-71.

[38] Tao C, Van DVJ, Cabau L, Montcada NF, Neutzner S, Srimath Kandada AR, et al. Fully solution-processed n-i-p-like perovskite solar cells with planar junction: how the charge extracting layer determines the open-circuit voltage. Adv Mater 2017;29(15):1604493.

[39] Azhar F, Lukas S-M, Germà G-B, Rajan J, Ivan M-S. Interfaces in perovskite solar cells. Adv Energy Mater 2017;7(22):1700623.

Highlights:

- Two low cost hexa-substituted benzene compounds are facile synthesized, in which dimethoxydiphenylamine groups are linked by fluorenyl or phenyl bridges attaching to the central benzene core.
- The additional flexible alkyl chains in the compounds influence the packing mode in solid state and the hole mobility.
- Perovskite solar cells employed these HTMs exhibit impressive PCEs of 15.9% and 16.7%, respectively, which are comparable to the reference cells based on spiro-OMeTAD.